Comparing the Excited-State Properties of a Mixed-Cation-Mixed-Halide Perovskite to Methylammonium Lead Iodide

Jan Brauer,[1]* Demetra Tsokkou,[1,2] Sandy Sanchez,[3] Nikolaos Droseros,[1,2] Bart Roose,[3] Edoardo Mosconi,[4] Xiao Hua,[3] Martin Stolterfoht,[5] Dieter Neher,[5] Ullrich Steiner,[3] Filippo De Angelis,[4,6] Antonio Abate,[3] Natalie Banerji[1,2]*

[1]Department of Chemistry, University of Fribourg, Chemin du Musée 9, CH-1700 Fribourg, Switzerland.

[2]Department of Chemistry and Biochemistry, University of Bern, Freiestrasse 3, CH-3012 Bern, Switzerland.

[3]Adolphe Merkle Institute, University of Fribourg, Chemin des Verdiers 4, CH-1700 Fribourg, Switzerland.

[4] Computational Laboratory for Hybrid/Organic Photovoltaics (CLHYO), Istituto CNR di Scienze e Tecnologie Chimiche "Giulio Natta" (CNR-SCITEC), Via Elce di Sotto 8, 06123 Perugia, Italy.

[5]Institute of Physics and Astronomy, University of Potsdam, Karl-Liebknecht-Str. 24-25, D-14476 Potsdam-Golm, Germany.

[6] Department of Chemistry, Biology and Biochemistry, University of Perugia, Via Elce di Sotto 8, 06123 Perugia, Italy.

***Corresponding authors**: jcbrauer@bluemail.ch, natalie.banerji@dcb.unibe.ch

Keywords: Perovskite solar cells, mixed-halide-mixed-cation composition, transient absorption spectroscopy, terahertz spectroscopy, DFT calculations, excited-state properties.

The Journal of Chemical Physics

Abstract

Organic-inorganic perovskites are one of the most promising photovoltaic materials for the design of next generation solar cells. The lead-based perovskite prepared with methylammonium and iodide was the first in demonstrating high power conversion efficiency, and it remains one of the most used materials today. However, perovskites prepared by mixing several halides and several cations systematically yield higher efficiencies than 'pure' methylammonium lead iodide ($MAPbI_3$) devices. In this work, we unravel the excited-state properties of a mixed-halide (iodide and bromide) and mixed-cation (methylammonium and formamidinium) perovskite. Combining time-resolved photoluminescence, transient absorption and optical-pump-terahertz-probe experiments with DFT calculations, we show that the population of higher-lying excited states in the mixed material increases the lifetime of photo-generated charge carriers upon above-bandgap excitation. We suggest that alloying different halides and different cations reduces the structural symmetry of the perovskite, which partly releases the selection rules to populate the higher-energy states upon light absorption. Our investigation thus shows that mixed halide perovskites should be considered an electronically different material than $MAPbI_3$, paving the way towards further materials optimization and improved power conversion efficiency of perovskite solar cells.

Introduction

Halide perovskites of ABX_3 composition consist of three main units, whereby A is either an organic or inorganic cation, B is a metal such as lead (Pb) or tin (Sn), and X is a halide. Each plays a unique role in defining the structural and photophysical properties of the perovskite.[1-5] Identifying optimal compositions has promoted organic-inorganic perovskites to being one of the most promising next generation photovoltaic (PV) materials,[6] and they have also proven themselves in efficient light emitting devices.[7] In addition to their high absorption coefficients, good transport properties and lack of intrinsic defects, optoelectronic tunability in perovskites can be achieved by substituting the chemical constituents of the basic units with mixtures of several cations or halides, allowing for example to absorb in different regions of the solar spectrum.[8, 9] The high performance achieved by single-halide-single-cation $MAPbI_3$ (methylammonium lead iodide perovskite, efficiency of 22.1%) already competes with existing PV technologies.[10] However, mixed-cation-mixed-halide perovskites have reached even higher efficiencies in single junction solar cells with records exceeding 23%,[11] and they show enhanced stability.[12-14] Although the superiority of the mixed perovskites is proven in terms of device performance, their excited-state properties remain largely unexplored,[15] leaving many open questions concerning the origin of their improved characteristics.[16] This is in stark contrast to the extensively investigated photophysics of $MAPbI_3$.[17-26] Since halide substitution is known to drastically affect the electronic structure and photophysics of perovskites,[27] we expect that alloying different halides might have strong implications on the optoelectronic nature and excited-state dynamics of the materials, which could be further enhanced by structural modifications caused by mixing both several halides and several cations.

In the present work, the excited-state properties are compared for $MAPbI_3$ and a mixed composition containing iodide and bromide as halides, as well as methylammonium (MA) and formamidinium (FA) cations ($(FA_{0.8}/MA_{0.2})Pb(I_{0.8}/Br_{0.2})_3$). This perovskite was chosen as

representative of the mixed-cation-mixed-halide family, due to its simpler composition compared to triple cation perovskites and its relatively high PV performance exceeding 20.8%.[11, 27-29] Combining time-resolved photoluminescence, transient absorption and optical-pump-terahertz-probe experiments with density functional theory (DFT) calculations, we relate the photophysics of the two perovskites to their electronic band structure. The carrier thermalization in the mixed perovskite is found to be significantly slower than in the pure one, which we attribute to the population of lower-lying valence bands (VBs) or higher-lying conduction bands (CBs), from where carriers relax slowly to the band-edge (~200 ps). Those higher excited states likely become accessible in the mixed perovskite due to structural distortions of the lattice that release the symmetry selection rules. We show that populating those higher-lying states with well above-bandgap excitation is beneficial in terms of increasing the carrier lifetime of the mixed perovskite compared to $MAPbI_3$.

Results and Discussion

Figure 1 shows the steady-state absorption spectra (expressed in terms of attenuation coefficient) and photoluminescence (PL) emission spectra of the pure $MAPbI_3$ and the mixed $(FA_{0.8}/MA_{0.2})Pb(I_{0.8}/Br_{0.2})_3$ perovskite. Overall, the absorption and emission spectra of the mixed perovskite is comparable to the one of pure $MAPbI_3$, except that their onset is slightly blue-shifted compared to the pure perovskite, indicating a higher optical band-gap for the mixed system compared to the pure one (1.6 eV versus 1.58 eV, as determined by the Tauc plot in Figure S1). Both materials display the typical absorption features spanning the whole visible spectrum with an absorption onset at ~760 nm and a shoulder at ~480 nm. DFT calculations including spin-orbit coupling also reveal an overall similar band structure for the two perovskites (Figure 1B and Figure S2). The lower energy transition around 760 nm is the direct band-gap transition from the valence band (VB) to the conduction band (CB) at the Γ

point of the Brillouin zone. The PL spectra of $MAPbI_3$ and $(FA_{0.8}/MA_{0.2})Pb(I_{0.8}/Br_{0.2})_3$ consist of a single emission band from the band gap peaking at 760 nm and 753 nm, respectively, and having in both cases a width of ~ 50 meV, supporting our working hypothesis that the mixed perovskite consists of a single phase and not a mixture of different phases.

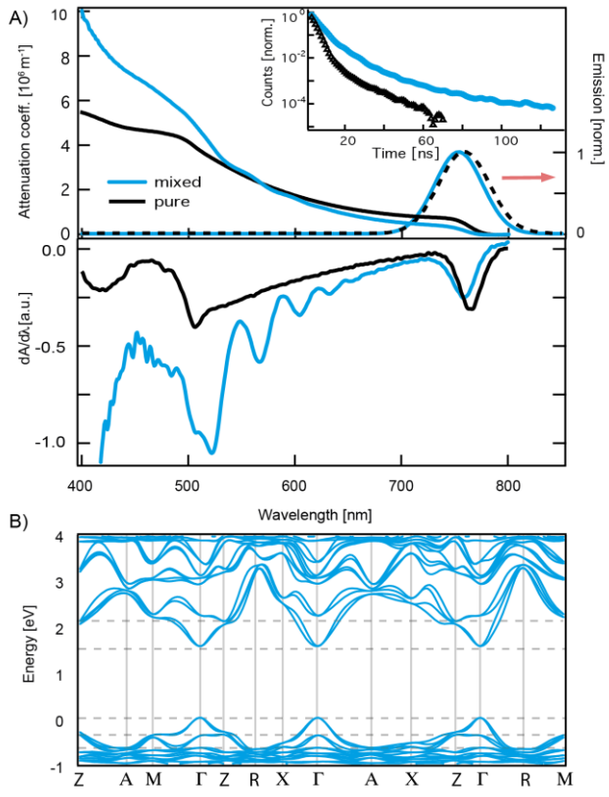

Figure 1. A) Upper panel: Attenuation coefficient spectra and photoluminescence (PL) emission spectra of pure $MAPbI_3$ and mixed $(FA_{0.8}/MA_{0.2})Pb(I_{0.8}/Br_{0.2})_3$ perovskites. The inset shows the PL emission lifetime upon excitation at 355 nm (with 1 μJ cm^{-2}). Grey lines represent theoretically obtained transitions for the mixed perovskite as detailed in Table 1. Lower panel: Derivative of the absorption spectra. B) Band structure of mixed $(FA_{0.8}/MA_{0.2})Pb(I_{0.8}/Br_{0.2})_3$ perovskite, as obtained by DFT calculations including spin-orbit coupling (SOC), for the most stable perovskite structure (see Methods for computational details).

Apart from the slightly blue-shifted bandgap in the mixed perovskite, a close look at the spectral shape reveals a progression of weak peaks between 500 nm and 650 nm, which are absent in pure $MAPbI_3$.This structure becomes more evident when looking at the derivative of

the absorption, as shown in the lower panel of Figure 1. The peak progression is present at the same wavelengths for a different film thickness (Figure S3), ruling out interference effects as its origin. Since this feature is absent in the spectra of pure $MAPbBr_3$ (Figure S4) and $MAPbI_3$ films and cannot be reproduced by their superposition, it represents an intrinsic property of the mixed material. According to the band structure obtained by the DFT calculations (Figure 1B and Figure S2), several lower-lying VBs and higher-lying CBs exist in both perovskites, and they can lead to direct transitions between the bands. In mixed $(FA_{0.8}/MA_{0.2})Pb(I_{0.8}/Br_{0.2})_3$, the valence band (VB1) is followed at lower energies (0.40 eV) by a well-defined VB2 and by a dense manifold of states (VB3) starting at 0.65 eV below VB1, all having maxima at Γ. The conduction band minimum (CB1) falls again at Γ, followed at higher energy by CB2, whose minimum is almost degenerate at Γ, M and Z. Table 1 summarizes the direct transitions between the mixed perovskite bands, as calculated from the band structure. The close match with the experimentally observed peak progression in the absorption spectrum points to the origin of the latter as a series of transitions to higher-lying states in the mixed perovskite. We suggest that alloying different halides and different cations reduces the structural symmetry of the perovskite, which partly releases the selection rules to populate the higher-energy states upon light absorption. Because of this, the progression of weak absorption peaks is only observed in the mixed $(FA_{0.8}/MA_{0.2})Pb(I_{0.8}/Br_{0.2})_3$ system, but not in pure $MAPbI_3$, in spite of their comparable band structure. This is consistent with the Rietveld refinements of the x-ray diffraction data (XRD) (Figure S5 and S6), which reveal tetragonal (*I*4/*mcm*) and trigonal (*P*3*m*1) crystal structures for the pure and mixed perovskite films, respectively. The main difference is a sizable shortening of the c-axis in the mixed perovskite (12.69 Å (pure) *vs.* 12.59 Å (mixed)), and negligible changes of a-/b- axes (both 8.89 Å, Table S1). Similar symmetry breaking of the unit cell has been recently reported by Selig et al for mixed halide perovskites.[30]

Table 1. Comparison between theoretical and experimental direct transitions for the mixed perovskite.

Transition	Theory (eV - nm)	Experiment (eV - nm)
VB1→CB1	1.58 - 785	1.6 – 775
VB2→CB1	1.98 -626	2.0 – 620
VB1→CB2	**2.16 - 574**	**2.1 – 590**
VB3→CB1	**2.23 -556**	**2.2 – 564**
VB2→CB2	2.56 - 484	2.4 – 517
VB3→CB2	**2.81 - 441**	**2.7 – 459**

Let us now turn to the excited-state dynamics of the pure and mixed perovskite. To ensure that the obtained results are not influenced by differences in samples characteristics, films of comparable morphology and thickness were used as confirmed by cross-section and top view scanning electron microscopy (SEM) images (Figure S7). For each material, all transient measurements shown here were performed on the same sample to ensure similar excitation conditions when the same incident pump fluence was used. In addition, measurements were performed at low fluences that correspond to initial excitation densities < 10^{17} cm^{-3} (except for the intensity-dependent measurements discussed below). Thus, any contribution to the excited-state dynamics arising from higher order recombination effects is negligible, allowing direct comparison between the different materials. It is important to mention that steady state and transient measurements were repeated on different sets of samples and similar results/conclusions were obtained. Time-resolved PL measurements (inset of Figure 1) using well above-bandgap excitation show that the carrier lifetime is substantially increased for the mixed $(FA_{0.8}/MA_{0.2})Pb(I_{0.8}/Br_{0.2})_3$ compared to $MAPbI_3$ (28 and 13 ns respectively, estimated from decay to 10^{-2}). The shape of the emission band does not change at different times after excitation, indicating the absence of inhomogeneous broadening caused by energetic disorder and supporting that there is no significant halide segregation,[31] which is also in agreement with the XRD data (Figure S5 and S6). We use femtosecond transient absorption (TA) spectroscopy to further elucidate the impact of using different cations and halides on the early relaxation

mechanisms and lifetimes of photogenerated charges. Results of the TA experiments for the mixed $(FA_{0.8}/MA_{0.2})Pb(I_{0.8}/Br_{0.2})_3$ perovskite upon excitation at 480 nm with a fluence of 0.7 $\mu J/cm^2$ are displayed in Figure 2A. Overall, the TA features in the mixed perovskite resemble the ones that have been reported for pure $MAPbI_3$ films,[23,32-37] which are shown for comparison in Figure S8. In brief, there are two negative signals that correspond to photobleaching transitions (PB1 at 500 nm and PB2 at 745 nm in the mixed perovskite). The PB2 signal is located at the band-edge and is therefore slightly blue-shifted in comparison to the pure perovskite (750 nm). The precise origin of PB1 in $MAPbI_3$ has been described in detail elsewhere,[23,32-37] and can be explained by a model comprising two CBs and two VBs. An alternative origin for this band could be the presence of a small amount of PbI_2,[38] however our DFT calculations and the similar dynamics between the PB1 and PB2 bands (Figure S8) support the assignment of PB1 to a perovskite transition. Nevertheless, our conclusions are not affected by the origin of this band. The broad positive feature between 500-720 nm is related to a photoinduced change in refractive index for $MAPbI_3$, and we assume a similar origin in $(FA_{0.8}/MA_{0.2})Pb(I_{0.8}/Br_{0.2})_3$.[39]

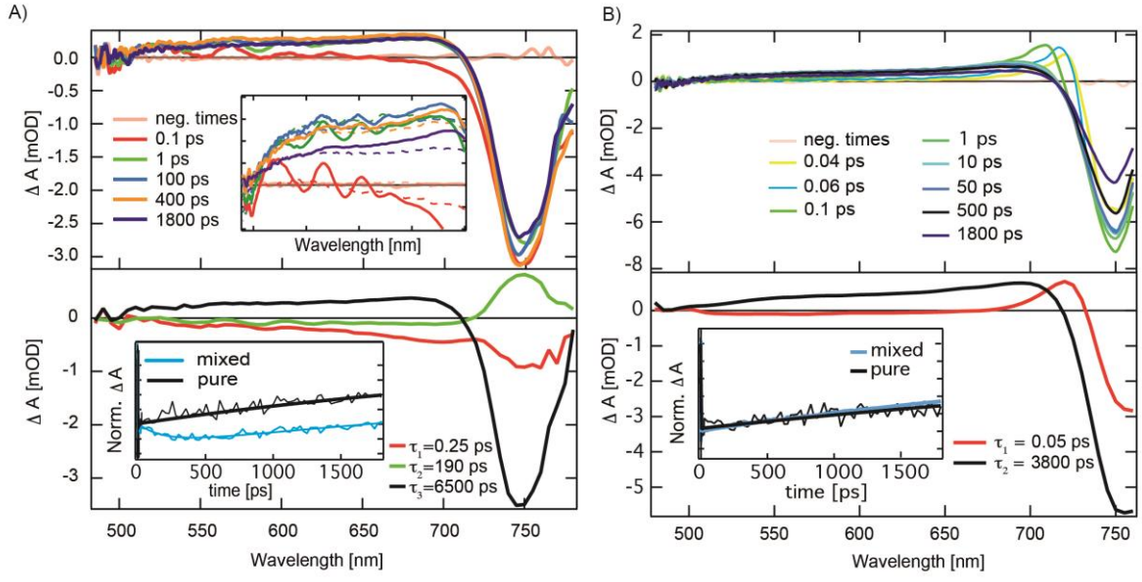

Figure 2. A) Selected transient absorption (TA) spectra (top) and decay-associated spectra (bottom) of the mixed $(FA_{0.8}/MA_{0.2})Pb(I_{0.8}/Br_{0.2})_3$ perovskite upon excitation at 480 nm with

0.7 μJ/cm^2. Inset upper panel: Zoom on the progression of peaks recorded at 3μJ/cm^2 (dotted lines are transient spectra of $MAPbI_3$ under identical excitation conditions for comparison). Inset lower panel: Normalized dynamics at the PB2 signal of $MAPbI_3$ and the mixed perovskite upon excitation at 480 nm. B) Selected TA spectra (top) and decay-associated spectra (bottom) of the mixed $(FA_{0.8}/MA_{0.2})Pb(I_{0.8}/Br_{0.2})_3$ perovskite upon excitation at 750 nm with 2.5 μJ/cm^2. Inset lower panel: Normalized dynamics at the PB2 signal of $MAPbI_3$ and the mixed perovskite upon excitation at 750 nm.

Exciting in the TA experiments at 480 nm leads to excess energy in the initially excited states. In both the pure and mixed perovskites, we observe on the sub-picosecond time scale a negative signal in the 650-720 nm region, which narrows rapidly into PB2, and which has been ascribed to thermally non-relaxed states (Figure 2A and Figure S8).[40] The early shape and evolution of the TA spectra of the pure perovskite have been analyzed in terms of a dynamic Burstein-Moss shift,[25] and by taking into account exciton and free charge contributions as well as carrier thermalization.[37] This ultrafast thermalization/relaxation is characterized by the decay-associated spectrum having a 0.25 ps and 0.32 ps time constant in the mixed and pure perovskite, respectively. Moreover, at 480 nm above-bandgap excitation, we expect population of a series of higher-lying excited states in $(FA_{0.8}/MA_{0.2})Pb(I_{0.8}/Br_{0.2})_3$, but not in $MAPbI_3$, as discussed above. This leads to three main differences in the TA results of the mixed compared to the pure perovskite films: i) The progression of peaks between 500 and 650 nm observed in the steady-state absorption spectrum, is present as well in the form of negative indents in the early TA spectra of only the mixed perovskite and disappears at time-delays longer than 500 ps (see inset Figure 2A upper panel). This confirms that the peaks are not due to interference effects in the thin film, but are related to bleaching of electronic transitions, in agreement with the theoretical predictions of Table 1. ii) An additional mechanism appears in the mixed perovskite, which is evident as a slow increase of PB2 seen in Figure 2A, and thus the maximum is reached hundreds of picoseconds after excitation. The corresponding rise of the dynamics by about 20% at 750 nm (and decay-associated spectrum with τ_2 = 190 ps) is absent

in the pure $MAPbI_3$ perovskite (Figure S8). Importantly, the rise of PB2 occurs simultaneously with the disappearance of the higher-energy oscillatory bleaching signals. We attribute the additional mechanism in the mixed composition, leading to the disappearance of the progression and rise of PB2 in ~200 ps, to the relaxation of carriers from higher-lying CBs or lower-lying VBs to the VB1/CB1 band-edge. TA measurements on the mixed perovskite were repeated using excitation at 540 nm (Figure S9) and similar long-lived oscillatory features were observed, since there is still enough excess energy to populate the higher-level states. iii) The slow recombination of the charges seen in the TA dynamics takes longer in the mixed perovskite (6500 ps) compared to pure $MAPbI_3$ (3600 ps), in agreement with the longer decay of the PL dynamics.

To evaluate the impact of populating the higher-lying states in the mixed perovskite, we repeated the TA experiments with excitation at 750 nm (Figure 2B), which induces initial excited states with little excess energy, allowing neither the population of the higher-energy states, nor thermally excited states within CB1 and VB1. Therefore, the sub-picosecond dynamics, present at 480 nm excitation in the mixed and the pure perovskite due to thermalization, is absent. Instead, there is an oscillatory feature overlaid with PB2, which has been previously assigned to excitons.[41, 42] The signature of excitons disappears within the first 50 fs in the mixed perovskite, while this takes about 100 fs in pure MAPbI3 (Figure S10). There is a concomitant rise of the positive TA signal in the 500-700 nm region (photoinduced reflectivity change due to free charges), which is much more pronounced in the pure perovskite. This points to a lower exciton binding energy in the mixed compared to the pure perovskite, leading to a higher ratio of directly generated free charges even at bandgap resonant excitation. The lower exciton binding energy might be related to the presence of FA, as has been shown by Galkowski et al. when substituting MA with FA cation in iodide perovskite.[43] Moreover, the signatures that we have identified with 480 nm excitation as evidence of higher energy

states accessible only in the mixed perovskite (progression of indents and spectral relaxation within ~200 ps) are not observed upon 750 nm excitation, because those states are not populated at the lower excitation energy. As a consequence, the TA dynamics can be analyzed globally using only two time constants, one for the exciton dissociation and one for the slow nanosecond recombination of the charges (Figure 2B, lower panel). We note that the recombination of charges is similar for $(FA_{0.8}/MA_{0.2})Pb(I_{0.8}/Br_{0.2})_3$ and $MAPbI_3$ with 750 nm excitation (inset of Figure 2B), indicating that the longer carrier lifetime in the mixed perovskite only exists with above-bandgap excitation. This is consistent with the similar PL decay with 730 nm excitation (Figure S11). The similar dynamics following excitation close to the band edge also reveal that there are no significant differences in the defect densities between the mixed and pure perovskites, otherwise different recombination rates would be observed even in the absence of excess excitation energy. This trend indicates that the charge recombination slows down for high excitation energies in the mixed perovskite, but not in the pure perovskite. Therefore, we infer that excitation into the higher valence and conduction bands of the mixed perovskite increases the lifetime of photogenerated carriers.

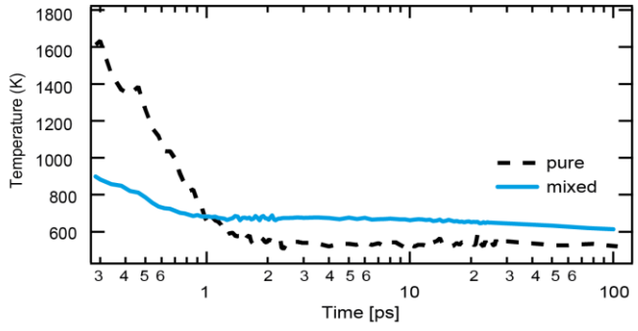

Figure 3. Carrier cooling curves for $MAPbI_3$ (dashed lines) and mixed $(FA_{0.8}/MA_{0.2})Pb(I_{0.8}/Br_{0.2})_3$ (solid lines) upon 480 nm excitation at 3 μJ/cm^2, obtained from the analysis of the TA spectra (see main text for details).

We have analyzed the hot carrier thermalization of the $(FA_{0.8}/MA_{0.2})Pb(I_{0.8}/Br_{0.2})_3$ and $MAPbI_3$ films upon excitation at 480 nm (with excess energy) using the model proposed by Beard et al.[37] A similar analysis has been previously applied to fit the TA spectra of various perovskites. .[37, 44, 45] To extract the carrier temperature as a function of time, we have thus approximated the Fermi-Dirac distribution for energies >> E_f with a Maxwell-Boltzmann distribution and have extracted the carrier temperature by fitting this to the TA spectra in the region between 640 and 730 nm (Figure S12). The carrier cooling curves are shown in Figure 3. At the used fluence of 3 $\mu J/cm^2$, the cooling of pure $MAPbI_3$ occurs mainly within 1 ps, according to thermalization within the excited energy band, as discussed above. Such a cooling rate is in agreement with previous TA measurements on halide perovskites performed at low pump fluences, for excitation energies where charge carriers have initially excess kinetic energy, and is dominated by the intrinsic Fröhlich charge carrier-phonon interaction.[37, 45, 46] The carrier cooling curve for the mixed perovskite is substantially different. The initial carrier temperature is lower than in the pure perovskite, which is reasonable since the high-energy photons will populate the higher-energy allowed states instead of directly generating hot carriers in CB1 or VB1. Therefore, a second slow cooling component of over 100 ps is present in addition to the sub-picosecond one. This slower carrier cooling component is compatible with an initial population of high-lying electronic states above the band gap and a subsequent relaxation to the band-edge of the mixed perovskite.[37] The relaxation leads to a population hot carriers in CB1 and VB1 on the hundreds of picosecond time scale, explaining the observed slower cooling at the band-edge transition. This attribution is supported by the fact that the slower cooling process occurs on a similar time scale as the rise of PB2 and the disappearance of the progression in the 500-650 nm region, which we assigned to the relaxation from the higher-energy states in the mixed perovskite.

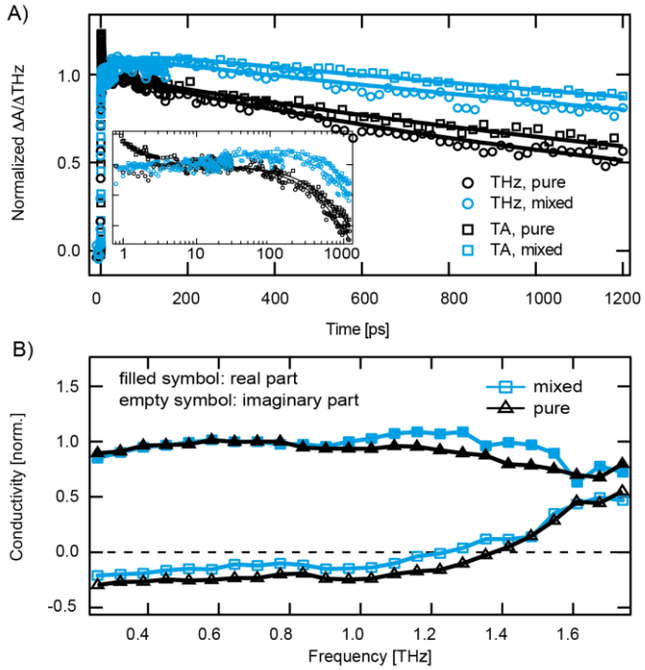

Figure 4. A) Normalized TA dynamics probed at PB2 (band-edge photo-bleach) compared to the THz photoconductivity dynamics for pure $MAPbI_3$ and mixed $(FA_{0.8}/MA_{0.2})Pb(I_{0.8}/Br_{0.2})_3$ upon photoexcitation at 480 nm (3 μJ/cm^2). Inset: Same data on a logarithmic time scale. B) Real ($\Delta\sigma_1$) and imaginary ($\Delta\sigma_2$) parts of THz photoconductivity spectra for $MAPbI_3$ and $(FA_{0.8}/MA_{0.2})Pb(I_{0.8}/Br_{0.2})_3$ obtained upon excitation at 480 nm with an absorbed pump fluence of ~ 3 μJ/cm^2 at a fixed pump-probe delay of 20 ps.

To further confirm our interpretations, the photoconductivity dynamics of the two perovskites were measured by optical-pump-terahertz-probe (OPTP) spectroscopy upon 480 nm excitation with 3 μJ/cm^2 (Figure 4A). While the TA dynamics is proportional only to the charge carrier population and relaxation, the THz photoconductivity dynamics is proportional to the product of the charge carrier density and their short-range mobility.[47] Interestingly, the mixed perovskite exhibits an initial rise of the THz dynamics reaching a maximum at about 100-200 ps after the excitation, similar to the dynamics of the band-edge carriers probed at PB2 in the TA measurements (Figure 4A). This reveals that the carriers probed in the THz measurements are essentially those that have relaxed to the band-edge energy levels, while the charges that populate the higher-lying CBs or lower-lying VBs are not visible due to the fact that they have a much lower mobility in these energy levels, so that their contribution to the conductivity is

insignificant. This is consistent with the band structure of the mixed perovskite obtained by DFT calculations (Figure S2). Notably, the band dispersion of VB2 and VB3 is much smaller than that of VB1 (lower slope when moving away from Γ), with VB2 showing an almost flat band along the Γ→Z direction. Similarly, CB2 exhibits a reduced slope along the Γ→Z direction than CB1. This implies higher carrier effective masses for transitions involving the secondary bands, especially VB2 and CB2, causing lower mobility in these bands. When reaching the band-edge after relaxation from the higher-lying states, the mobility of the carriers thus increases and leads to a rise of the THz photoconductivity dynamics in the mixed $(FA_{0.8}/MA_{0.2})Pb(I_{0.8}/Br_{0.2})_3$ perovskite. This is not observed in pure $MAPbI_3$ (Figure 4A), because the higher states are not populated and the thermalization to the band-gap occurs on the sub-ps timescale, which is not accessed via THz spectroscopy. In the case of the pure perovskite, there is a difference between the TA and THz dynamics at early times (up to 5 ps), which suggests a fast increase of the charge carrier mobility. As carrier cooling is ultrafast in this material (sub-ps time scale at low fluences), the weak decay observed in the TA dynamics during the first few ps can be attributed to some trap recombination, while the difference between the TA and THz dynamics indicates that the carrier mobility concomitantly increases. We suggest that this is caused by the depopulation of the band edge energy levels, leading to lower carrier density. Similar results have been previously obtained in the pure perovskite via time dependent complex THz photoconductivity measurements.[48]

The complex THz photoconductivity spectra of the pure and mixed perovskite are shown Figure 4B at a pump-probe delay of 20 ps. At this longer time delay, and because the charge carriers in the higher-lying CBs and lower-lying VBs in the mixed perovskite do not show significant THz response due to their high effective mass, the photoconductivity spectrum reflects mainly carriers at the band-edge. The sub-micrometer size of the perovskite crystals used in this study (Figure S7) leads to important backscattering of charges at the crystal

boundaries, which explains deviation from the Drude behavior in the photoconductivity spectra. Thus, for both perovskites, a positive almost flat real part of the photoconductivity ($\Delta\sigma_1$) is seen, while the imaginary part ($\Delta\sigma_2$) is negative for low frequencies (indicating carrier localization due to disorder)[48, 49] and becomes positive at higher frequencies. There is no significant change in the shape of the spectra between the two materials, indicating a similar degree of localization of the charge carriers at the band-edge and thus confirming the similar grain sizes observed by SEM images in mixed and pure perovskite films.

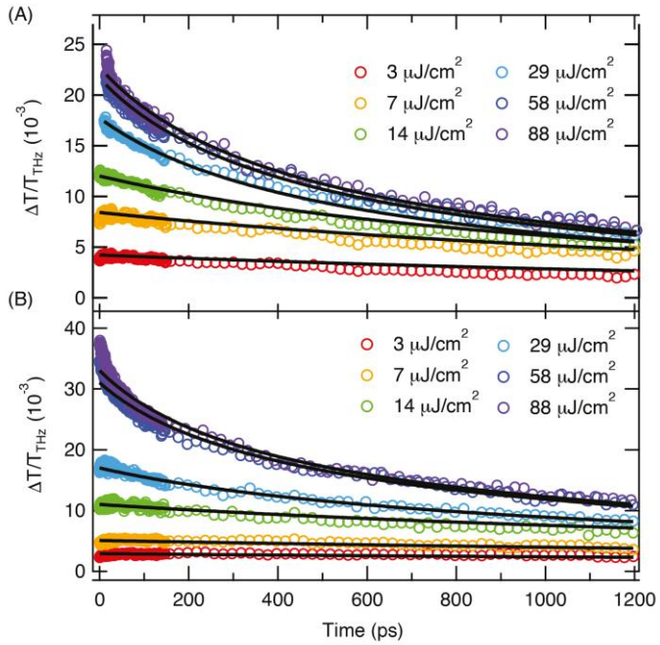

Figure 5. Temporal evolution of the THz photoconductivity (transmission difference at the maximum THz signal with and without pump at different pump-probe time delays) for A) $MAPbI_3$ and B) $(FA_{0.8}/MA_{0.2})Pb(I_{0.8}/Br_{0.2})_3$ using excitation at 480 nm and several pump fluences between 3-88 μJ/cm^2. The solid lines represent the simultaneous fit of the decay curves with a differential rate equation (equation 1).

Finally, we have investigated the recombination mechanism in the pure and mixed perovskite (with excess energy excitation at 480 nm), by analyzing the decay of the THz photoconductivity dynamics as a function of excitation density (Figure 5). We note that this decay at different fluences is similar to the one probed by TA spectroscopy in the PB2 band (Figure S13), confirming that the THz dynamics indeed reflect the loss of carrier population

due to recombination and that the charge carrier mobility is not significantly modified in the time window measured here. We have shown in the analysis of the TA measurements that (short-lived) excitons only play a role with band-edge excitation at 750 nm, so that we see here at 480 nm excitation mainly recombination of free charges. The THz photoconductivity decay becomes gradually faster with photoexcited carrier density, since higher order recombination processes take place at higher fluences, such as second-order bimolecular and third-order Auger recombination. [20, 25, 50] On the other hand, the photoconductivity dynamics at low pump fluences becomes independent of the charge density and is related to monomolecular processes (most likely trap-assisted recombination).[50] A differential rate equation that describes the temporal evolution of the charge density *n(t)* was simultaneously fit to the decay curves at all fluences, in order to extract the rate constants for the different recombination processes:

$$\frac{dn(t)}{dt} = -k_1 n(t) - k_2 n^2(t) - k_3 n^3(t) \qquad \textit{(equation 1)}$$

Here, k_1 is the monomolecular recombination rate constant associated with trap recombination, k_2 is the bimolecular coefficient arising from band-to-band electron-hole recombination and k_3 is the Auger coefficient, which is a non-radiative recombination process and involves the participation of three charges. Since we are focusing here on recombination, we only included decay components in the analysis and neglected the weak signal rise due to relaxation to the band-edge in the mixed perovskite, which becomes masked by the important decay amplitude caused by fast higher-order recombination effects as the fluence increases. We set the monomolecular rate constant k_1 to be equal to the long-lived component found via TA measurements at the lowest pump fluence, while the initial photoexcited carrier density was deduced from the steady-state absorbance at 480 nm, the sample thickness (~450 nm), and assuming a penetration depth of ~330 nm. The rate constants for the pure and mixed perovskite are summarized in Table 2. Due to the similarity between the TA and THz dynamics at the different pump fluences (Figure S13), comparable higher order recombination coefficients

would be extracted via both methods. The values found for the higher order rate constants in $MAPbI_3$ are on the same order of magnitude as those previously reported.[51, 52] However, both k_1 (monomolecular trap recombination) and k_2 (bimolecular electron-hole recombination) are significantly lower in the mixed compared to the pure perovskite, evidencing reduced recombination in $(FA_{0.8}/MA_{0.2})Pb(I_{0.8}/Br_{0.2})_3$. This is consistent with the longer carrier lifetimes seen with above-bandgap excitation in the femtosecond TA measurements and nanosecond time-resolved PL measurements. We have shown that the morphology, crystal size and trap density are similar in the mixed and pure perovskite and that the extended lifetime in the mixed perovskite correlates with the population of higher excited states (seen only with excitation well above the band gap). We therefore tentatively ascribe the reduced recombination to the presence of carriers in higher-lying CBs and lower-lying VBs during the first 200 ps after photo-excitation, that have lower mobility (reducing bimolecular encounter). The charge carriers need a longer time to reach the band-edge from the higher populated CBs and VBs (~200 ps), before undergoing bimolecular and trap-based recombination. During that time, the carriers already present in CB1/VB1 can move away and further reduce the probability of bimolecular encounter. Another factor that could affect the higher order recombination coefficients is the presence of a hot-phonon bottleneck, shown to be significant in halide perovskites.[37, 44, 45] In $MAPbI_3$, the charge carriers are photoexcited to the CB1/VB1 levels with high excess kinetic energy that they lose by phonon emission. On the other hand, in mixed $(FA_{0.8}/MA_{0.2})Pb(I_{0.8}/Br_{0.2})_3$, the charge carriers populate higher energy CBs and VBs in which they have less excess energy, since they will occupy states close to the edge of the bands, reducing the density of emitted phonons and leading to a weaker hot-phonon bottleneck effect compared to the pure perovskite. Therefore, it is unlikely that this effect accounts for the slower higher-order recombination in the mixed material.

Table 2. Global fitting rate constants of monomolecular, bimolecular and Auger recombination are given for $MAPbBr_3$, $MAPbI_3$ and FA/MAPbI/Br.

	k_1 ($\times 10^8$ s^{-1})	k_2 ($\times 10^{-10}$ cm^3 s^{-1})	k_3 ($\times 10^{-28}$ cm^6 s^{-1})
$MAPbI_3$	2.8	3.3	1.2
$(FA_{0.8}/MA_{0.2})Pb(I_{0.8}/Br_{0.2})_3$	1.5	1.4	1.0

In conclusion, we have compared here the excited-state properties of single-halide-single-cation $MAPbI_3$ and mixed-halide-mixed-cation $(FA_{0.8}/MA_{0.2})Pb(I_{0.8}/Br_{0.2})_3$. We find significant differences in their photophysics. The mixed perovskite is characterized by a reduced exciton binding energy, longer free charge carrier lifetime, and reduced trap and bimolecular recombination. The enhanced carrier lifetime and reduced recombination correlate with the population of higher excited states (involving higher-lying CBs or lower-lying VBs) with above-bandgap excitation, which lead to characteristic signatures in the steady-state and transient absorption spectra. We suggest that alloying different cations and anions reduces the structural symmetry of the perovskite, enabling the otherwise forbidden transitions to the higher electronic states. The mobility of the carriers in the higher-lying CBs or lower-lying VBs is lower (according to terahertz measurements and the computed band structure) than at the band-edge. The carrier lifetime is reduced in pure $MAPbI_3$, where those states are not accessible, and when $(FA_{0.8}/MA_{0.2})Pb(I_{0.8}/Br_{0.2})_3$ is excited without excess energy at the band-edge resonant transition. As summarized in Figure 6, for above-bandgap excitation, the photogenerated charges relax to the band-edge on a significantly longer time scale in the mixed (180 ps) than in the pure (sub-ps) perovskite, due to the involvement of the higher states. We note that a similar band structure for the pure perovskite has previously been suggested.[32, 53] Since electron and hole transfer to the selective contacts within perovskite solar cells may occur from energy states above the band-edge,[54, 55] the charge extraction in such devices might benefit from the relatively slow cooling to the band-edge in the mixed perovskite.

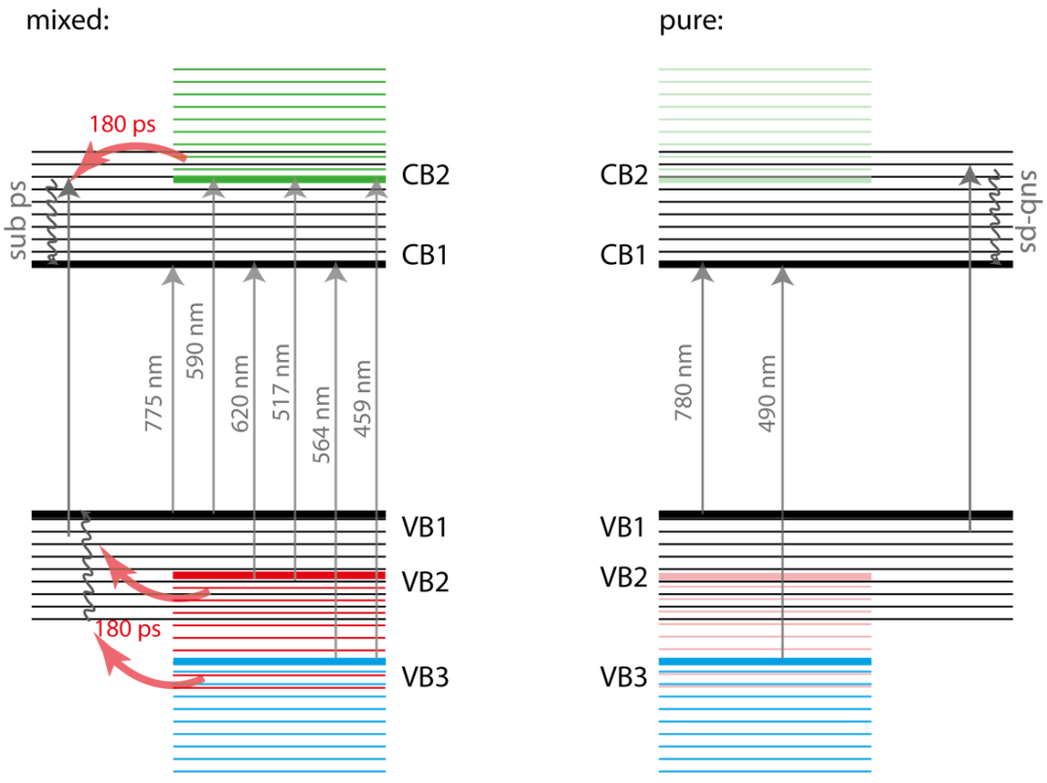

Figure 6. Schematic representation of the proposed band structure, absorption transitions and excited-state relaxation mechanisms for the mixed and pure perovskite. In the mixed perovskite, the population of CB2, VB2 and VB3 increases the lifetime of the photogenerated carriers.

Supporting Information

Experimental methods and additional figures as mentioned in the text.

Acknowledgements

J.B., D.T., N.D. and N.B. thank the University of Fribourg, the University of Bern and the Swiss National science Foundation (grants PP00P2_15036, and National Competence Center for Research NCCR-MUST: Molecular Ultrafast Science and Technology), for financial support. A.A., U.S., S.S. and B.R. acknowledge the Adolphe Merkle Institute and the Swiss National Science Foundation [Program NRP70 No. 153990]. The Ministero dell'Istruzione dell'Università e della Ricerca (MIUR) and Università degli Studi di Perugia are acknowledged

for financial support through the program "Dipartimenti di Eccellenza 2018-2022" (Grant AMIS) to F.D.A. E.M. acknowledges the European Union's Horizon 2020 research and innovation program under Grant Agreement No. 764047 of the ESPRESSO project.

References

[1] G. Giorgi, J.-I. Fujisawa, H. Segawa, and K. Yamashita, The Journal of Physical Chemistry C 118 12176 (2014).

[2] P. N. Rudd, and J. Huang, Trends in Chemistry 1 394 (2019).

[3] C. Tablero Crespo, Solar Energy Materials and Solar Cells 195 269 (2019).

[4] G. E. Eperon, S. D. Stranks, C. Menelaou, M. B. Johnston, L. M. Herz, and H. J. Snaith, Energy & Environmental Science 7 982 (2014).

[5] J. T.-W. Wang, Z. Wang, S. Pathak, W. Zhang, D. W. deQuilettes, F. Wisnivesky-Rocca-Rivarola, J. Huang, P. K. Nayak, J. B. Patel, H. A. Mohd Yusof, Y. Vaynzof, R. Zhu, I. Ramirez, J. Zhang, C. Ducati, C. Grovenor, M. B. Johnston, D. S. Ginger, R. J. Nicholas, and H. J. Snaith, Energy & Environmental Science 9 2892 (2016).

[6] EPLI, A White Paper from the European Perovskite Initiative. (2019).

[7] S. Das, S. Gholipour, and M. Saliba, Energy & Environmental Materials 2 146 (2019).

[8] S. A. Kulkarni, T. Baikie, P. P. Boix, N. Yantara, N. Mathews, and S. Mhaisalkar, Journal of Materials Chemistry A 2 9221 (2014).

[9] Y. Zhou, Y.-H. Jia, H.-H. Fang, M. A. Loi, F.-Y. Xie, L. Gong, M.-C. Qin, X.-H. Lu, C.-P. Wong, and N. Zhao, Advanced Functional Materials 28 1803130 (2018).

[10] J. Cao, B. Wu, R. Chen, Y. Wu, Y. Hui, B.-W. Mao, and N. Zheng, Advanced Materials 30 1705596 (2018).

[11] A. K. Jena, A. Kulkarni, and T. Miyasaka, Chemical Reviews 119 3036 (2019).

[12] O. J. Weber, B. Charles, and M. T. Weller, Journal of Materials Chemistry A 4 15375 (2016).

[13] A. Binek, F. C. Hanusch, P. Docampo, and T. Bein, The Journal of Physical Chemistry Letters 6 1249 (2015).

[14] X. Zhang, H. Liu, W. Wang, J. Zhang, B. Xu, K. L. Karen, Y. Zheng, S. Liu, S. Chen, K. Wang, and X. W. Sun, Advanced Materials 29 1606405 (2017).

[15] G. Pang, X. Lan, R. Li, Z. He, and R. Chen, Nanoscale 11 5215 (2019).

[16] A. Solanki, P. Yadav, S.-H. Turren-Cruz, S. S. Lim, M. Saliba, and T. C. Sum, Nano Energy 58 604 (2019).

[17] J. Even, L. Pedesseau, and C. Katan, Journal of Physical Chemistry C 118 11566 (2014).

[18] Q. Lin, A. Armin, R. C. R. Nagiri, P. L. Burn, and P. Meredith, Nature Photonics 9 106 (2015).

[19] A. Miyata, A. Mitioglu, P. Plochocka, O. Portugall, J. T.-W. Wang, S. D. Stranks, H. J. Snaith, and R. J. Nicholas, Nature Physics 11 582 (2015).

[20] M. Saba, M. Cadelano, D. Marongiu, F. Chen, V. Sarritzu, N. Sestu, C. Figus, M. Aresti, R. Piras, A. G. Lehmann, C. Cannas, A. Musinu, F. Quochi, A. Mura, and G. Bongiovanni, Nature Communications 5 5049 (2014).

[21] N. Sestu, M. Cadelano, V. Sarritzu, F. Chen, D. Marongiu, R. Piras, M. Mainas, F. Quochi, M. Saba, A. Mura, and G. Bongiovanni, The Journal of Physical Chemistry Letters 6 4566 (2015).

[22] S. D. Stranks, G. E. Eperon, G. Grancini, C. Menelaou, M. J. P. Alcocer, T. Leijtens, L. M. Herz, A. Petrozza, and H. J. Snaith, Science 342 341 (2013).

[23] G. Xing, N. Mathews, S. Sun, S. S. Lim, Y. M. Lam, M. Grätzel, S. Mhaisalkar, and T. C. Sum, Science 342 344 (2013).

[24] V. D'Innocenzo, G. Grancini, M. J. P. Alcocer, A. R. S. Kandada, S. D. Stranks, M. M. Lee, G. Lanzani, H. J. Snaith, and A. Petrozza, Nature Communications 5 1 (2014).

[25] J. S. Manser, and P. V. Kamat, Nature Photonics 8 737 (2014).

[26] A. Filippetti, P. Delugas, and A. Mattoni, The Journal of Physical Chemistry C 118 24843 (2014).

[27] H. F. Zarick, N. Soetan, W. R. Erwin, and R. Bardhan, Journal of Materials Chemistry A 6 5507 (2018).

[28] N. J. Jeon, J. H. Noh, W. S. Yang, Y. C. Kim, S. Ryu, J. Seo, and S. I. Seok, Nature 517 476 (2015).

[29] D. Bi, W. Tress, M. I. Dar, P. Gao, J. Luo, C. Renevier, K. Schenk, A. Abate, F. Giordano, J.-P. Correa Baena, J.-D. Decoppet, S. M. Zakeeruddin, M. K. Nazeeruddin, M. Grätzel, and A. Hagfeldt, Science Advances 2 e1501170 (2016).

[30] O. Selig, A. Sadhanala, C. Müller, R. Lovrincic, Z. Chen, Y. L. A. Rezus, J. M. Frost, T. L. C. Jansen, and A. A. Bakulin, Journal of the American Chemical Society 139 4068 (2017).

[31] V. D'Innocenzo, A. R. S. Kandada, M. De Bastiani, M. Gandini, and A. Petrozza, Journal of the American Chemical Society 136 17730 (2014).

[32] A. Marchioro, in *Department of Chemistry* (EPFL, 2014).

[33] L. Wang, C. McCleese, A. Kovalsky, Y. Zhao, and C. Burda, Journal of the American Chemical Society 136 12205 (2014).

[34] K. G. Stamplecoskie, J. S. Manser, and P. V. Kamat, Energy & Environmental Science 8 208 (2015).

[35] O. Flender, J. R. Klein, T. Lenzer, and K. Oum, Physical Chemistry Chemical Physics 17 19238 (2015).

[36] T. C. Sum, N. Mathews, G. Xing, S. S. Lim, W. K. Chong, D. Giovanni, and H. A. Dewi, Accounts of Chemical Research 49 294 (2016).

[37] Y. Yang, D. P. Ostrowski, R. M. France, K. Zhu, J. van de Lagemaat, J. M. Luther, and M. C. Beard, Nature Photonics 10 53 (2016).

[38] T. J. Jacobsson, J.-P. Correa-Baena, E. Halvani Anaraki, B. Philippe, S. D. Stranks, M. E. F. Bouduban, W. Tress, K. Schenk, J. Teuscher, J.-E. Moser, H. Rensmo, and A. Hagfeldt, Journal of the American Chemical Society 138 10331 (2016).

[39] M. B. Price, J. Butkus, T. C. Jellicoe, A. Sadhanala, A. Briane, J. E. Halpert, K. Broch, J. M. Hodgkiss, R. H. Friend, and F. Deschler, Nature Communications 6 8420 (2015).

[40] H.-Y. Hsu, C.-Y. Wang, A. Fathi, J.-W. Shiu, C.-C. Chung, P.-S. Shen, T.-F. Guo, P. Chen, Y.-P. Lee, and E. W.-G. Diau, Angewandte Chemie International Edition 53 9339 (2014).

[41] J. C. Brauer, Y. H. Lee, M. K. Nazeeruddin, and N. Banerji, Journal of Materials Chemistry C (2016).

[42] G. Grancini, A. R. Srimath Kandada, J. M. Frost, A. J. Barker, M. De Bastiani, M. Gandini, S. Marras, G. Lanzani, A. Walsh, and A. Petrozza, Nature Photonics 9 695 (2015).

[43] K. Galkowski, A. Mitioglu, A. Miyata, P. Plochocka, O. Portugall, G. E. Eperon, J. T.-W. Wang, T. Stergiopoulos, S. D. Stranks, H. J. Snaith, and R. J. Nicholas, Energy & Environmental Science 9 962 (2016).

[44] J. Yang, X. Wen, H. Xia, R. Sheng, Q. Ma, J. Kim, P. Tapping, T. Harada, T. W. Kee, F. Huang, Y.-B. Cheng, M. Green, A. Ho-Baillie, S. Huang, S. Shrestha, R. Patterson, and G. Conibeer, Nature Communications 8 14120 (2017).

[45] J. Fu, Q. Xu, G. Han, B. Wu, C. H. A. Huan, M. L. Leek, and T. C. Sum, Nature Communications 8 1300 (2017).

[46] H. Kawai, G. Giorgi, A. Marini, and K. Yamashita, Nano Letters 15 3103 (2015).

[47] M. C. Beard, G. M. Turner, and C. A. Schmuttenmaer, Physical Review B 62 15764 (2000).

[48] C. La-o-vorakiat, T. Salim, J. Kadro, M. T. Khuc, R. Haselsberger, L. Cheng, H. X. Xia, G. G. Gurzadyan, H. B. Su, Y. M. Lam, R. A. Marcus, M. E. Michel-Beyerle, and E. E. M. Chia, Nature Communications 6 7903 (2015).

[49] N. V. Smith, Physical Review B 64 155106 (2001).

[50] M. B. Johnston, and L. M. Herz, Accounts of Chemical Research 49 146 (2016).

[51] Y. Yang, M. J. Yang, Z. Li, R. Crisp, K. Zhu, and M. C. Beard, Journal of Physical Chemistry Letters 6 4688 (2015).

[52] R. L. Milot, G. E. Eperon, H. J. Snaith, M. B. Johnston, and L. M. Herz, Advanced Functional Materials 25 6218 (2015).

[53] B. Anand, S. Sampat, E. O. Danilov, W. Peng, S. M. Rupich, Y. J. Chabal, Y. N. Gartstein, and A. V. Malko, Physical Review B 93 161205 (2016).

[54] J. C. Brauer, Y. H. Lee, M. K. Nazeeruddin, and N. Banerji, Journal of Materials Chemistry C 4 5922 (2016).

[55] G. Xing, B. Wu, S. Chen, J. Chua, N. Yantara, S. Mhaisalkar, N. Mathews, and T. C. Sum, Small 11 3606 (2015).

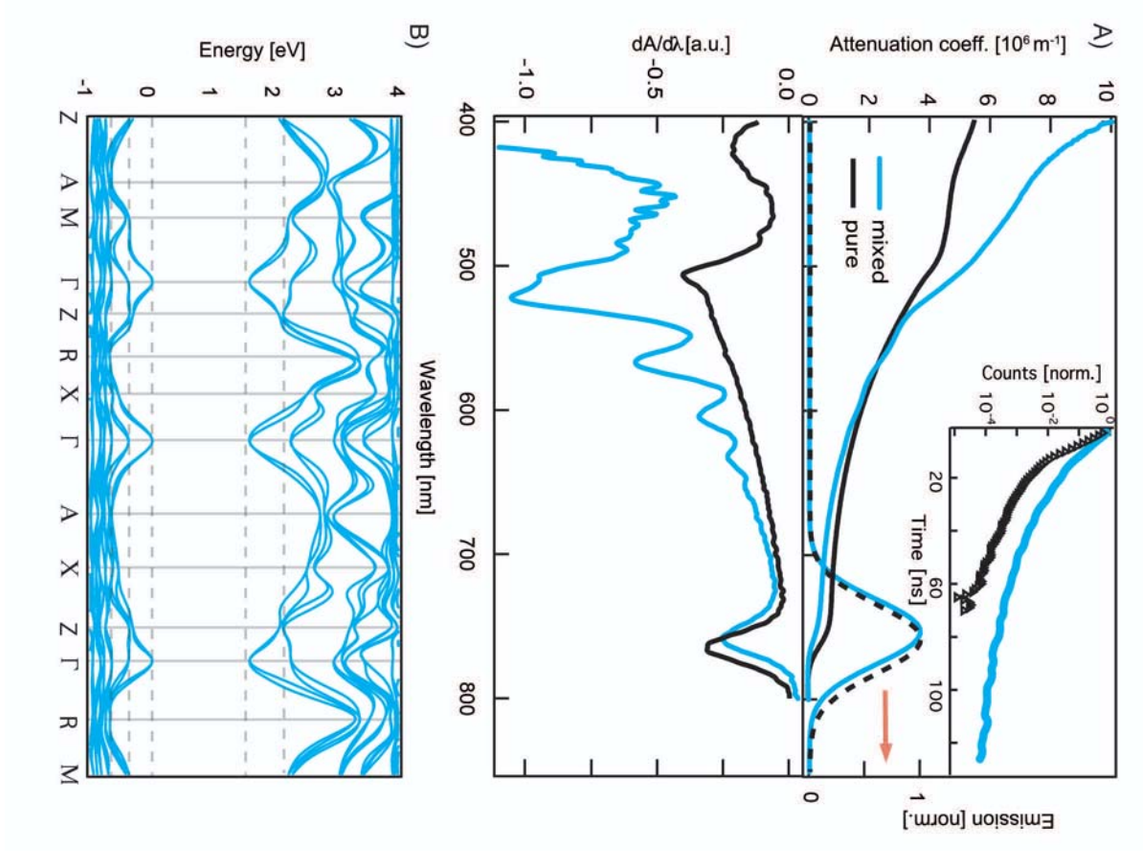

PLEASE CITE THIS ARTICLE AS DOI: 10.1063/1.5133021

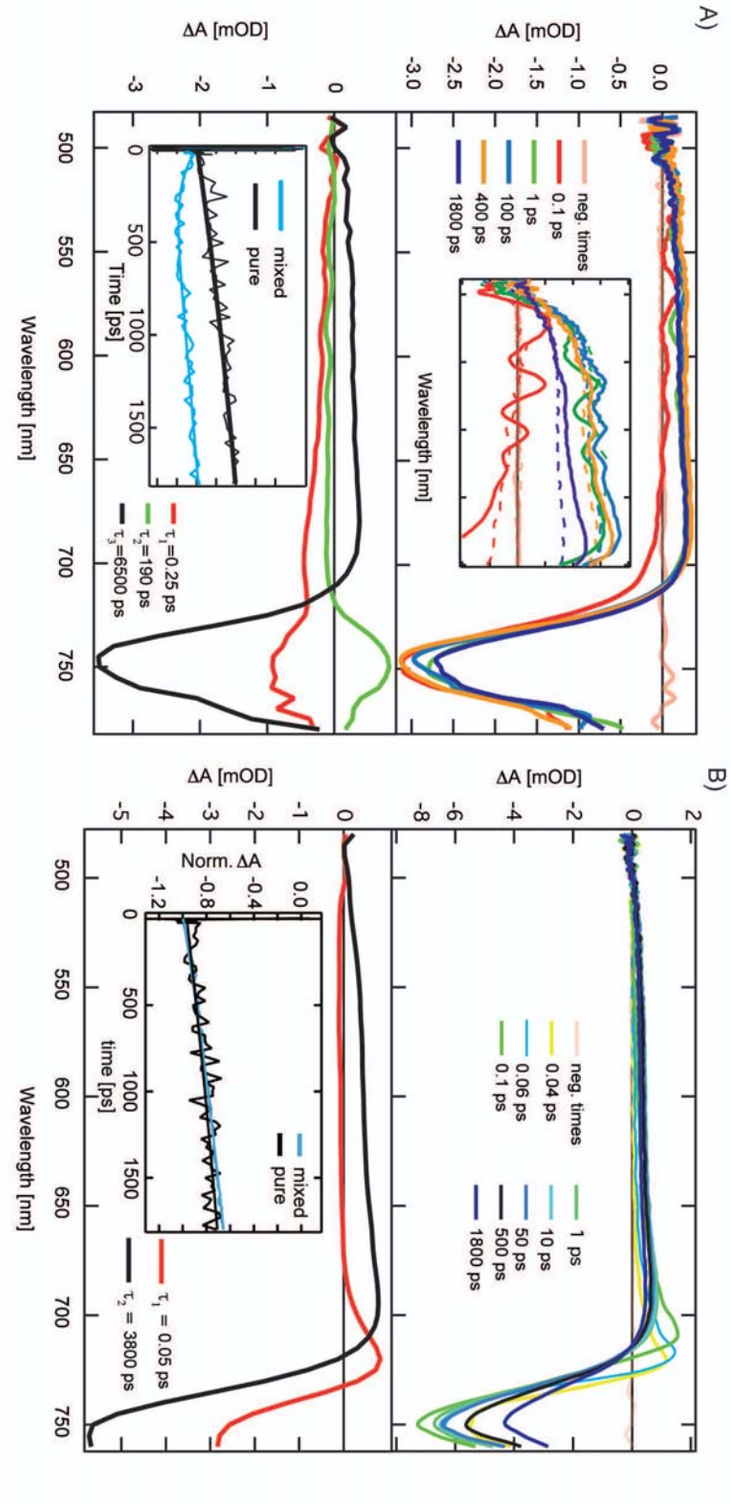

PLEASE CITE THIS ARTICLE AS DOI: 10.1063/1.5133021

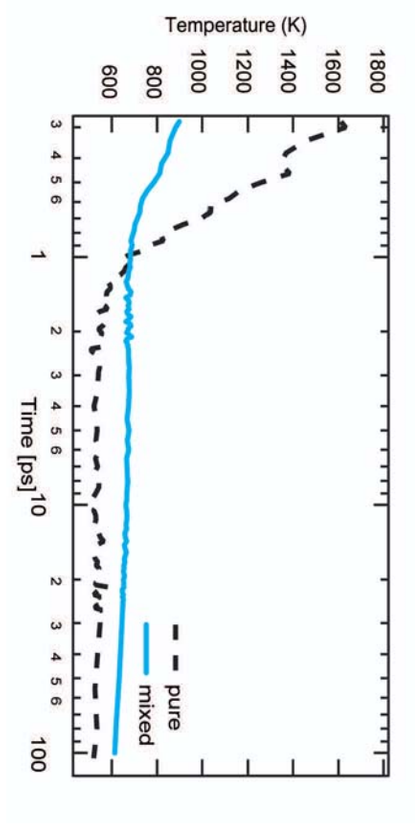

PLEASE CITE THIS ARTICLE AS DOI: 10.1063/1.5133021

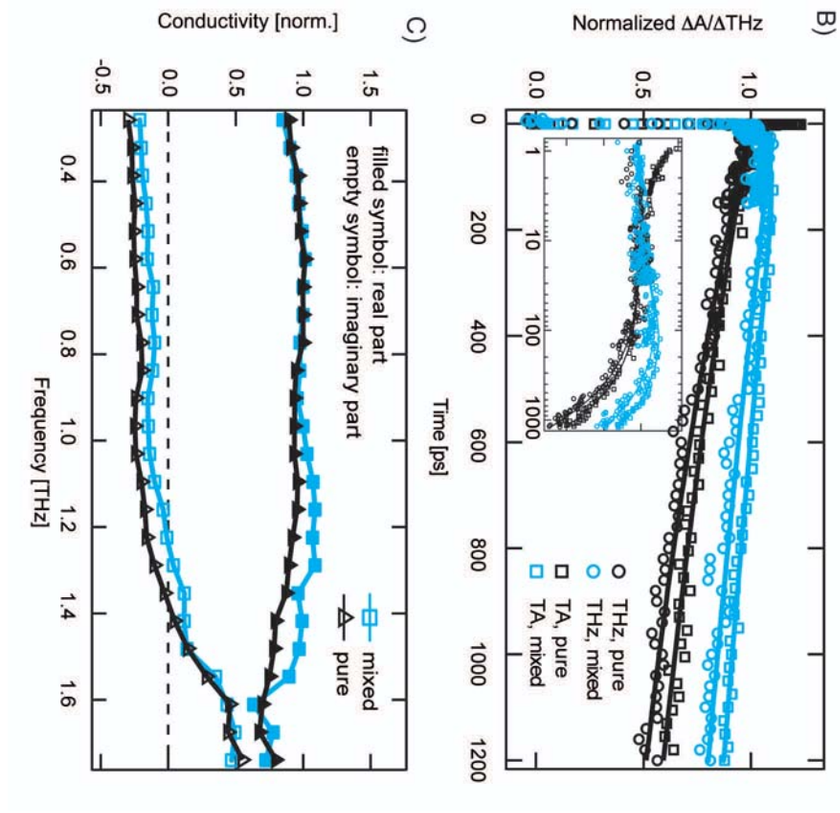

PLEASE CITE THIS ARTICLE AS DOI: 10.1063/1.5133021